IEEE Access
Multidisciplinary : Rapid Review : Open Access Journal

Received 6 November 2023, accepted 11 November 2023, date of publication 14 November 2023, date of current version 17 November 2023.

Digital Object Identifier 10.1109/ACCESS.2023.3332689

RESEARCH ARTICLE

A Real-Time Prognostic-Based Control Framework for Hybrid Electric Vehicles

LAXMAN TIMILSINA[1], (Graduate Student Member, IEEE), PHUONG H. HOANG[2], (Member, IEEE), ALI MOGHASSEMI[1], (Graduate Student Member, IEEE), ELUTUNJI BURAIMOH[1], (Member, IEEE), PHANI KUMAR CHAMARTHI[1], (Member, IEEE), GOKHAN OZKAN[1,3], (Senior Member, IEEE), BEHNAZ PAPARI[1,4], (Senior Member, IEEE), AND CHRISTOPHER S. EDRINGTON[1], (Senior Member, IEEE)

[1]Real-Time COntrol and Optimization Laboratory (RT-COOL), Holcombe Department of Electrical and Computer Engineering, Clemson University, Clemson, SC 29634, USA
[2]Operation Technology Inc., Irvine, CA 92618, USA
[3]Dominion Energy Innovation Center, Clemson University, North Charleston, SC 29405, USA
[4]Department of Automotive Engineering, Clemson University, Greenville, SC 29607, USA

Corresponding author: Laxman Timilsina (ltimils@clemson.edu)

This work was supported by Clemson University's Virtual Prototyping of Autonomy Enabled Ground Systems (VIPR-GS) under Cooperative Agreement with the U.S. Army DEVCOM Ground Vehicle Systems Center (GVSC) under Grant W56HZV-21-2-0001.

ABSTRACT The increasing popularity of electric vehicles is driven by their compatibility with sustainable energy goals. However, the decline in the performance of energy storage systems, such as batteries, due to their degradation puts electric vehicles and hybrid electric vehicles at a disadvantage compared to traditional internal combustion engine vehicles. This paper presents a prognostic-based control framework for hybrid electric vehicles to reduce the cost of operating hybrid electric vehicles by considering the degradation of energy storage systems. The strategy utilizes a degradation forecasting model of electrical components to predict their degradation pattern and uses the prediction to control hybrid electric vehicles via their energy management systems to reduce the degradation of components. A real-time controller hardware-in-the-loop is set up to run the proposed strategy. An hybrid electric vehicle model is developed on Typhoon (i.e., a real-time simulator), which is connected to two layers, energy management and degradation forecasting layer, deployed in Raspberry Pis, respectively. All these components are communicated through CAN communication, where the actual operating condition of the vehicle is sent from Typhoon to each Raspberry Pis to implement the proposed control strategy. With this approach, the cost of operating hybrid electric vehicles can be reduced, making them more competitive than their combustion engine counterparts shown in both numerical simulations and the CHIL experiment.

INDEX TERMS Battery degradation, degradation abatement, degradation modeling, Markov chain model, remaining useful life, battery life prediction, controller hardware-in-loop, state of health.

ACRONYMS

Q_{rem}	Remaining Capacity of Battery.
BEV	Battery Electric Vehicle.
CAN	Controller Area Network.
CHIL	Controller Hardware-in-Loop.
DF	Degradation Forecasting.
DoD	Depth of Discharge.
DP	Dynamic Programming.
ECU	Electronic Control Unit.
EM	Energy Management.
ESS	Energy Storage System.
EV	Electric Vehicle.
GHG	Green House Gases.
HEV	Hybrid Electric Vehicle.
HF	Hybridization Factor.

The associate editor coordinating the review of this manuscript and approving it for publication was Yu Liu.

HIL	Hardware-in-Loop.
HMI	Human-Machine Interface.
ICE	Internal Combustion Engine.
PBCF	Prognostic-based Control Framework.
PHEV	Plug-in Hybrid Electric Vehicle.
PMP	Pontryagin's Minimum Principle.
RTDS	Real-time Digital Simulator.
SC	Supercapacitor.
SNL	Sandia National Laboratory.
SoC	State of Charge.
SoH	State of Health.
V2G	Vehicle-to-Grid.
V2V	Vehicle-to-Vehicle.

I. INTRODUCTION

The increasing concern over greenhouse gas (GHG) emissions and their detrimental effects on the environment, as well as the implementation of strict emission regulations by governments worldwide, has led to the replacement of conventional internal combustion engine (ICE) vehicles with electrified vehicles. This shift towards electrified vehicles, along with improvements in renewables [1], is also driven by the need to address environmental pollution, petroleum product cost fluctuations, and supply and demand issues [2]. Electric vehicles (EVs) like battery electric vehicles (BEV), hybrid electric vehicles (HEVs), and plug-in hybrid electric vehicles (PHEV) are becoming the preferred mode of transportation as they combat severe environmental pollution and reduce the use of petroleum products. Although EVs emit zero emissions, their widespread adoption is hindered by range anxiety and limited public charging infrastructure [3]. In contrast, HEVs combine the benefits of traditional ICEs with those of electric motors and batteries, providing adequate vehicle mileage while achieving significant fuel-saving improvements.

The widespread use of EVs is currently constrained by a number of issues, despite its advantages. Power electronics are particularly important and need to be improved to improve EV efficiency and reliability [4]. Costs associated with energy storage, charging infrastructure, and the dependability of electrical sources throughout operation are a few of these restrictions [5]. Among these, the energy storage system (ESS) expenses are viewed as a key barrier to the competitiveness of electric cars compared to gasoline-powered vehicles. Among different ESSs, Li-ion batteries are emerging as the best fit for EVs as well as for other applications, as they have a higher energy density than any other battery technologies [6], [7]. A typical 30% of an EVs overall cost is attributed to battery costs as of 2020 [8]. The economic feasibility of electric cars is put into question by this. Reducing the costs associated with ES systems' deterioration is essential to expedite electrified transportation deployment.

The presence of multiple energy-generating sources in HEVs demand for energy management (EM) [9], [10]. The objective of the EM is to distribute the power demanded by the vehicles among ICE and other ESSs by reducing the overall fuel consumption [11]. Recently, several research has been done to improve the optimization function of the EM. EM techniques can be broadly classified into four main categories: predictive control method, learning method, heuristic method, and globally optimum approach [12]. Utilizing globally optimal methods can lead to minimum fuel consumption when provided with complete information regarding future power demand [3], [13]. Among different algorithms, dynamic programming (DP) and Pontryagin's minimum principle (PMP) are the most commonly used algorithms [11], [14], [15], [16]. The primary limitations of DP implementation are the curse of dimensionality and the considerable computing overhead required. Although several DP approximation techniques can alleviate the computational burden, they are still unsuitable for real-time EM problem-solving [11], [17]. And, for PMP, the iterative nature of the two-point boundary value problem (TPBVP) arising from it leads to longer computation times [18]. The non-convex nature of the optimization problem makes achieving global optimality in distributed energy management a challenging task in current research [19]. A dual-objective approach for distributed energy management is proposed in [20]. The approach involves two distinct steps. In the initial phase, several requirements of the EM optimization problem are relaxed to employ a method that converges to global optimality. The findings of the first stage are then utilized to modify the constraints of the overall optimization problem. The algorithm used in EM impacts the degradation of the battery [21]. This paper presents the utilization of a constrained EM algorithm, which is straightforward to implement in real-time applications. The objective of this algorithm is to minimize fuel consumption and is explained in detail in Sections II and IV-A3, respectively.

The components used in a vehicle degrade with time due to the vehicle's operation. As a result, these components' output is compromised, which could make the vehicle's operation unreliable. One of these components is the ESS utilized in EVs and HEVs. Compared to a gasoline-powered car, the initial cost of an electrified vehicle is typically higher. Nearly 30% of the overall cost of the vehicle goes toward ESS [8]. The ESS degradation raises concerns regarding electrified vehicles' system dependability and viability. As a result, there will be a significant impact on economic goals from ES deterioration. Li-ion batteries are proving to be the most suitable ESS for EV applications due to their superior energy density compared to other battery technologies. They have higher power density, good high-temperature performance, and, most crucially, they are lighter and smaller, so they are considered a promising choice for EVs [22].

The degradation of the battery results in a decrease in its capacity, and when the capacity drops below 80%, the reliability of the vehicle's operation becomes questionable [22]. This implies that the battery's operating range should be between 100% (initial capacity) and 80% for the vehicle to operate dependably. After the battery drops to 80% of its initial capacity, the battery needs to be replaced [22]. However, replacing the battery would significantly increase the vehicle's operational costs, making it an uneconomical option.

The degradation of the battery used in HEV can be minimized by controlling the power supplied by the battery to the vehicle, which is allocated by the EM. According to [23], the techniques used by the EM impact the rate at which the battery of an HEV degrades. This observation supports the idea that EM is crucial in controlling the power from multiple power-generating sources in the vehicle. The literature suggests that various operational factors, such as temperature, depth of discharge, charging, and discharging currents, influence a battery's degradation. Therefore, it is advisable to consider operational conditions while modeling the degradation of electrical components [24]. Thus, the EM can be considered a viable option for preventing or reducing component degradation. However, incorporating operating conditions that degrade the battery faster into the objective function of an EM is difficult because the primary objective of an EM is to minimize the vehicle's fuel consumption.

There have been several research in developing an algorithm for an EM that can reduce the degradation of the battery. Recently, there has been a growing concern about component degradation, and several works have addressed this issue by adding degradation costs to the EM's objective function. For example, in [25], a linear degradation cost is added to the EM's objective function, while in [26], the degradation rate of a component is estimated from empirical data and used to construct an objective cost for the component considering degradation, investment, and fuel consumption costs. Similarly, in [27], the degradation cost is added to the EM's objective function for different sources used in a microgrid to minimize the degradation of the components.

Similarly, various studies have followed another approach to minimize the degradation of batteries used in HEVs. Study [28] proposed a supercapacitor (SC) in addition to the battery for the minimization of degradation of the battery. Under this architecture, in extreme conditions (i.e., when there is a high power demand), SC supplies the power so that the degradation of the battery is minimized. However, this requires an additional device, i.e., SC, which increases the vehicle's cost and additional control objectives. Similarly, in study [29], a cost-minimization model, a predictive control problem, is formulated to balance fuel consumption and battery degradation. This problem considers fuel consumption, electricity costs associated with battery charging/discharging, and the equivalent battery degradation cost. To address the computational complexity of this optimization, the continuation/generalized minimal residual (C/GMRES) algorithm is employed to determine the expected engine power command in real-time. However, this study does not consider the factors that accelerate the degradation mechanism in the battery.

The safe and reliable operation of EVs heavily relies on the condition of the battery. However, Li-ion-based EV batteries are inherently limited by aging, which results in complex degradation over the battery's lifetime. Consequently, the battery's capacity decreases over time, leading to a reduced driving range [22]. The task of predicting the degradation pattern is challenging due to the scarcity of battery data used in automotive applications. Generating such data is difficult, expensive, and time-consuming and is often kept confidential by the automobile industry. Some studies use battery cell degradation data from various laboratories, as presented in [30], to predict future values using data-driven methods. The degradation process of a battery is a complex phenomenon and is dependent on its current state and operating conditions. To overcome these challenges, methodologies combining different operating condition data can provide more information on degradation patterns with higher accuracy [31]. Also, study [32] proposes a combined data-driven method using a convolution neural network (CNN), convolutional block attention module (CBAM), and long short-term memory (LSTM) neural network to predict the degradation pattern of the battery.

A. STATEMENT OF CONTRIBUTIONS

The contributions of this paper can be summed up as follows. A prognostic-based control framework (PBCF) for HEVs is proposed and examined. Firstly, a degradation forecasting (DF) layer is proposed to predict the degradation rate of the battery used in HEV. In the DF layer, Markov chain-based model is introduced to predict the degradation rate of the battery. It utilizes a multi-state model to model the states of the battery, which are load-dependent and based on the battery cell data obtained from the Sandia National Laboratory (SNL) [33]. Secondly, it emphasizes real-time degradation abatement in HEV. The proposed degradation abatement strategy (i.e., PBCF) involves integrating the DF layer into the existing EM as an upper layer. The DF's predicted result (i.e., the degradation rate cost) is used to adjust the EM's optimization problem to reduce the battery's degradation without compromising the vehicle's functioning. The proposed strategy can be applied to other applications, such as DC microgrids, as done in [5]. Finally, the proposed strategy is validated through numerical simulations and controller-hardware-in-the-loop (CHIL) experimentation, demonstrating the proposed strategy's cost-saving benefits.

Also, this study expands upon the findings of the conference paper by highlighting the cost-saving benefits of the proposed strategy by incorporating real-time controller CHIL experimentation alongside numerical simulations.

The remainder of the paper is structured in the following manner: Section II discusses the problem and the motivation behind the proposed strategy. Section III explains the vehicle architecture considered in this study. Section IV introduces the PBCF and the degradation prediction. The effectiveness of the proposed framework is evaluated through numerical simulations in Section V. Section VI presents a CHIL experiment to validate the proposed approach further. Finally, Section VII provides the paper's conclusion and suggests future research directions.

II. PROBLEM FORMULATION

Consider a series HEV consisting of an ICE and an ESS, i.e., a battery supplying the power the vehicle demands for its operation. Here, due to the presence of multiple power-generating sources in the vehicle, it demands EM. The utilization of EM in HEVs is common due to their ability to save fuel [13]. However, it is important to note that various powertrain configurations may require different optimization formulations for EM, resulting in different strategies. In the case of a series HEV shown in Fig. 1 (explained in detail in Section III), the optimization of EM can be generally presented as follows:

$$\min \sum_{s \in \mathcal{S}} f_s\big(P_s(t_k)\big) \tag{1a}$$

$$P_s(t_k) \in \mathcal{P} \tag{1b}$$

$$x_s(t_k) \in \mathcal{X} \tag{1c}$$

where t_k is the time instant in the discrete domain, $\mathcal{S}$ is the set of indices of energy sources, and $P_s(t_k)$ is power generated by source s at t_k, $x_k(t_k)$ is the set of states of system s, and $\mathcal{P}$ and $\mathcal{X}$ are correspondingly the constraints set of $P_s(t_k)$ and $x_k(t_k)$. A more comprehensive explanation of this EM is provided in Section IV-A3, where additional constraints that must be satisfied, as denoted by (14), (15), and (16), respectively are explained in detail. For the sake of presentation, t_k is omitted.

The main goal of this EM is to efficiently distribute power between the power-generating sources to achieve economic objectives while also taking into account the limitations of the system [34]. Energy management (EM) focuses on minimizing fuel consumption as an economic objective. It aims to achieve this goal by allocating more power to the battery, especially under ideal battery conditions.

However, fuel cost is not only the vehicle's operating cost; the degradation of the components should also be included in the vehicle's operating cost. For example, when more power is allocated to the battery by the EM to reduce fuel consumption, the battery starts to degrade faster as the battery has to supply a larger current [22]. This will make the operation of the vehicle uneconomical as the battery needs to be replaced faster, and the battery is one of the expensive components of the vehicle.

Therefore, the following two observations can be summarized from the EM's optimization problem:

- Observation 1: EM looks into the vehicle's operating condition and calculates the power references to be supplied by the multiple sources into the vehicle.
- Observation 2: The amount of power supplied by the sources or operating condition of the components impacts its degradation process. The higher the power supplied or power flow from the source or components, the higher the degradation rate. For example, in batteries, the higher the amount of charging/discharging current, the higher the degradation [22].

Over time, the capacity of components decreases due to degradation, and different components may degrade at different rates. As a result, it is essential to factor in degradation costs when optimizing operating costs based on the degradation rate of the components. Energy management can help regulate component degradation to satisfy vehicle load demands.

The following section explains the architecture of the HEV model considered in this project. Then in Section IV, a PBCF approach is proposed that predicts component degradation rate, which is then incorporated into the optimization problem of energy management to determine optimal operation costs while accounting for degradation costs. Therefore, this study presents a method for predicting the degradation of components used in a HEV. The predicted degradation is utilized to find the degradation cost and to modify the objective function of the EM given by (1a), which aims to minimize component degradation.

III. ELECTRICAL MODEL OF HYBRID ELECTRIC VEHICLE

HEVs are becoming increasingly popular as they offer a more sustainable solution to transportation. HEVs use multiple energy sources to provide propulsion power, with at least one of them delivering electrical energy to drive an electric motor. HEVs can be classified into different types depending on the energy sources and the architecture used to deliver the power. The most common type of HEV uses an ICE and a battery as a source of power to meet the vehicle's power demands. Depending on how ICE and an electric motor contribute to a vehicle's transmission, HEVs can be classified into different architectures, such as series hybrid, parallel hybrid, series-parallel hybrid, and complex hybrid [35].

This paper considers a series hybrid architecture due to its simplicity and flexibility in control. The ICE is not connected directly to the drivetrain in a series HEV. Instead, its output is converted into electricity via a generator. The electricity generated is then used to either charge a battery or power an electric motor that drives the vehicle's wheels. This configuration allows for greater control over the power delivered to each wheel, simplifying traction control. Fig. 1 shows a configuration of a series HEV, which includes an engine and battery as power generating sources. Using power electronics technology has greatly improved the efficiency and reliability of HEVs. The series hybrid architecture offers several benefits, including improved fuel efficiency, reduced emissions, and greater control over the power delivered to each wheel. Furthermore, the absence of a direct link between the ICE and the drivetrain provides increased control flexibility and simplifies traction control.

A brief discussion of the electrical model is presented here. The model houses a 600 V_{DC} bus powered by an ICE and an ESS. As can be seen in the figure, energy sources and loads are decoupled from the bus by the power

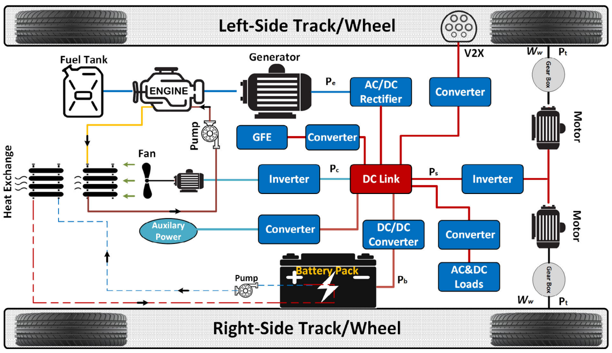

FIGURE 1. Series HEV powertrain configuration considered in this paper.

electronics converters interface. This design is economically feasible because of recent advancements in power electronics and reduced power electronic device costs. Because of the decoupling, the implementation of EM is eased as the issues of power split in HEVs are relaxed. In particular, this design allows various constraints in EM due to the dynamics of propulsion loads and the ICE to be relaxed. This design also allows the vehicle-to-grid (V2G) mode and the vehicle-to-vehicle (V2V) mode. Thus, the design contains a V2X outlet.

The series HEV model considered in this project is developed based on the power flow equation of the vehicle and deployed in MATLAB/Simulink and the real-time digital simulator (RTDS) Typhoon HIL 606 in Sections V and VI, respectively. No vehicle dynamics are considered to ease the complexity of the vehicle. The vehicle is driven by a predefined US06 drive cycle. All the parameters of the HEV needed to find the propulsion power using Ansys Motor-CAD for the US06 drive cycle are used from study [36]. The battery's state of charge (SoC) is mathematically based on the amount of power it supplies to the vehicle as allocated by the EM.

$$i_{bat} = \frac{P_{bat}}{V_{dc}} \tag{2a}$$

$$\dot{SoC}_{bat} = \begin{cases} -\dfrac{1}{\eta_{coul}} \dfrac{i_{bat}(t)}{Q_{norm}} & \text{if } i_{bat}(t_k) < 0 \\ -\eta_{coul} \dfrac{i_{bat}(t)}{Q_{norm}} & \text{if } i_{bat}(t_k) > 0 \end{cases} \tag{2b}$$

where P_{bat} is the power allocated by the EM to be supplied by the battery, V_{dc} is the DC link voltage which is assumed to be constant to $600V$, η_{coul} is the Coulombic efficiency or charge efficiency, which accounts for charge losses and depends on current operating conditions [37], and Q_{norm} is the nominal capacity of the battery.

The initial SoC of the battery is considered to be 80% and the SoC is varied between predefined boundaries of lower and upper limits of 40% and 80% for the efficient operation of the battery as shown by (3).

$$\underline{SoC_{bat}} \leq SoC_{bat} \leq \overline{SoC_{bat}} \tag{3}$$

IV. DEGRADATION FORECASTING AND PROGNOSTIC BASED CONTROL FRAMEWORK

In this section, a framework for degradation forecasting and abatement is presented. Certain aspects of [5] are discussed to provide a complete understanding. Nonetheless, this work represents an advancement over [5]. Specifically, this section provides a more elaborate discussion of the proposed strategy and emphasizes that the objective of the proposed strategy is to minimize the total degradation costs. The complete steps for the proposed system in this study are illustrated in Fig. 2. In this section, each step in this figure is explained in detail under each subsection.

The decreasing cost and increasing capability of computational devices have enabled the widespread use of power electronic devices in vehicles, making it easier to implement computationally intensive algorithms and strategies for efficient vehicle operation [38]. This includes optimization and forecasting functionalities essential for effective vehicle control. In this section, a hierarchical control strategy (shown in Fig. 3) with an upper layer to an EM layer of DF is introduced, and the operation of each layer is explained in detail. This multilevel control strategy takes advantage of the developments in computational technology, allowing for cost-effective and efficient vehicle operation.

In this multilevel control architecture, the first layer is the DF layer, which uses Markov's chain degradation model to predict component degradation. The second layer is the energy management (EM) layer, which allocates the power to the sources in the HEV. The final layer is where the HEV model is deployed. Section IV-A explains the degradation modeling and prediction technique used in this study, Section IV-A3 explains the reconfiguration of the EM optimization objective based on the output from the DF layer, and Section III has previously discussed the HEV model configuration.

A. DEGRADATION MODELING AND PREDICTION

In every system, components degrade over time, some degrading faster than others based on their robustness and application. In HEV, there are several components whose life cycle count decreases once the vehicle is in operation. However, this study is focused on the degradation of the power-generating sources present in the HEVs. While ICEs can also degrade, batteries are particularly prone to it. This study focuses on battery degradation since HEVs with high hybridization factors (HF) are used nowadays. This means batteries with higher capacity are used and can cost up to 30% of the price of the entire vehicle, as mentioned previously.

In automotive applications, the battery's life cycle is shorter than other components, and it is considered unreliable to operate after it reaches 80% of its initial capacity. The initial cost of a battery is high, so it is necessary to have a longer life for the operation of the vehicle to be economically viable. A battery's lifetime depends on its operation and degradation rate, which is a complex mechanism. Battery degradation is a significant limiting factor in battery lifetime; thus, it is

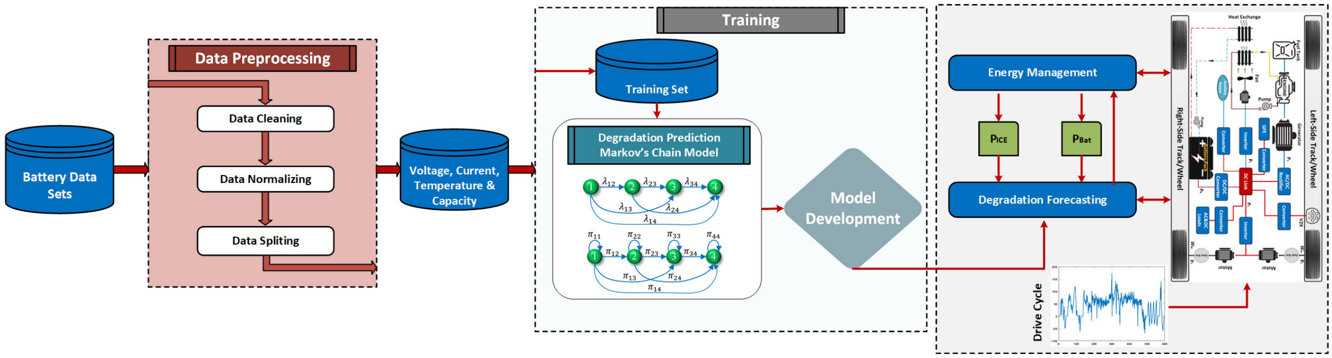

FIGURE 2. Overall schematic diagram of the proposed system.

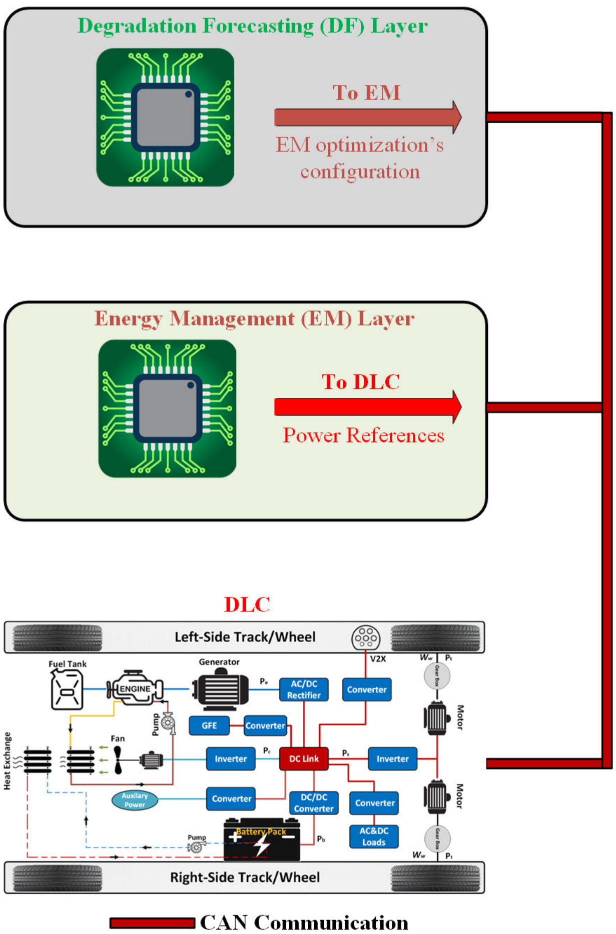

FIGURE 3. Hierarchical control architecture.

essential to investigate this mechanism thoroughly and reduce it to extend the battery's lifetime.

Several factors stimulate battery degradation, and predicting the degradation rate of a battery is a demanding task due to the complex nature of the process. However, it is crucial to determine the degradation pattern to ensure reliable operation and timely maintenance. Identifying the factors that accelerate the aging process can help to minimize the degradation process. The most common factors that affect battery capacity and give rise to degradation are temperature, discharging current, charging current, and depth of discharge (DoD) [22], [39]. These parameters have impacts depending on the mode of operation of the battery or vehicle. When the battery or vehicle is in operation, all these factors have different effects on the battery and result in degradation [40]. The impact on the battery is severe if it is fully discharged compared to when it's discharged from 100% to 60% [41]. The battery in EVs is subjected to various stress due to these extreme factors. This can be verified from Fig. 4 and Fig. 5, respectively, which show the impact of temperature and discharging/charging current on the degradation pattern of a battery for different cell data obtained from SNL [33]. Among these factors, the charging and discharging current have a more severe impact on the degradation pattern of the battery, which is further elaborated in the study [42].

Based on Fig. 4, it is evident that an increase in temperature leads to a faster degradation of battery cells. Specifically, the battery cell operating at 35°C exhibits the most rapid degradation compared to the cells at 15°C and 25°C. This trend holds true when the battery operates at lower temperatures as well. The battery data set analyzed in this study corresponds to the findings presented in [22] regarding the impact of temperature on the degradation of a battery. Likewise, Fig. 5 demonstrates that higher charging/discharging currents result in accelerated battery degradation based on the battery data set considered in this study. The chemical mechanisms inside the battery responsible for this degradation are explained in detail in [22]. In Fig. 4 and Fig. 5, occasional spikes occur at specific intervals, giving the impression of a potential capacity recovery. However, it's important to note that these spikes are not indicative of any data recovery phenomenon. Instead, they result from the system restarting during the data acquisition process.

Based on the above observations, a degradation model that is dependent on load is utilized. The model uses a Markov chain and comprises four states to predict the degradation process of a component, which is explained in the upcoming Section IV-A1. Markov chain is a valuable algorithm for anticipating future outcomes. One merit of

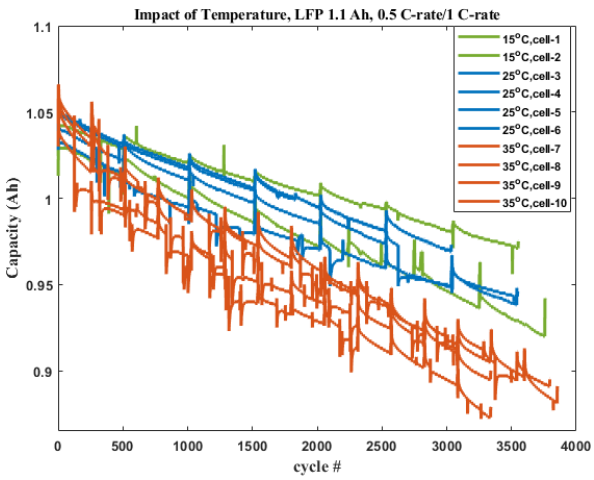

FIGURE 4. Impact of temperature on battery degradation for different cells.

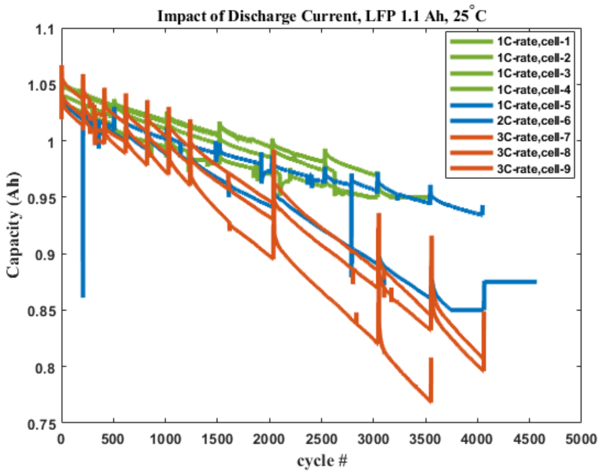

FIGURE 5. Impact of discharge/charge current on battery degradation for different cells.

leveraging these tools lies in their simplistic design, making them easily understandable to multiple user levels, even those with no background in statistical methods. Apart from their approachability feature, these models boast flexibility regarding modeling various nuances. They can integrate diverse inputs such as historical data, which significantly enhance precision towards future predictions. Markov chain models also possess commendable computational efficiency acting as a considerable strength concerning substantial data systems management requirements- particularly in real-time applications calling for rapid and precise prognoses. Consequently, this technique's wide-ranging adaptability, teamed with speed and ease of use, secure its applicability across multiple applications.

1) MARKOV CHAIN BASED DEGRADATION MODEL

The binary model is widely used to represent a system as either a working or failing state because of its simplicity and computational efficiency. However, the multistate model is often used instead of a binary model to provide a more accurate representation of the system. This increases the granularity of the multistate model. A model with 4 states is chosen as a compromise between precision and complexity because increasing the number of states can lead to a more complex and computationally demanding model.

In various studies, components have been represented using a multi-state model with four states to represent the system accurately. For instance, a component has been represented using four states as perfect, useful, pseudo-fault, and fault in [43]. Similarly, transformers have been described using four states, namely good, fair, poor, and very poor, in study [44]. In [45], drivetrain components of wind turbines have been represented by normal working, degraded, critical, and functional failure states. Moreover, in [27], different power-generating sources in microgrids have been defined as four states denoted by the number 1,2,3,4. In line with these studies, the present study also follows a multistate model where four states are defined based on a component's degradation signal $d_s^e(t_k)$, which represents the capacity loss of the component. Where, $d_s^e(t_k)$ represents the degradation signal of source s at time t_k which is the sum of actual degradation $d_s^a(t_k)$ and the error of the estimation $\sigma_s(t_k)$ represented as follow:

$$d_s^e(t_k) = d_s^a(t_k) + \sigma_s(t_k) \tag{4}$$

The assumptions for the degradation are formally stated as follows:

Assumption

1) There is no improvement in the degradation of a component between two consecutive maintenance or repair times.
2) The maximum of the actual degradation $d_s^a(t_k)$ is 1.
3) Between two consecutive maintenance or repair times, the actual degradation $d_s^a(t_k)$ exhibits a monotonically decreasing behavior.

The degradation signals in study [27] were converted into 4 states by dividing the range of signals into intervals and assigning each interval a specific state. Similarly, this study also adopts 4 states, namely perfect, good, degraded, and unreliable, each represented by a maximum capacity. The conversion of degradation signals into states is defined in the following points. Additionally, batteries used in automotive applications, are typically used from 100% to 80%. Therefore, this study defines four states based on the remaining capacity (Q_{rem}) of the battery ($\rho_x = Q_{rem}$), as follows:

- State 1 (Perfect): The hard constraint for this state is $d_s^a(t_k) \geq \rho_1$. For the battery, $\rho_1 = 90\%$.
- State 2 (Good): The hard constraint for this state is $\rho_1 \geq d_s^a(t_k) \geq \rho_2$. For the battery, $\rho_1 = 90\%$ and $\rho_2 = 85\%$.
- State 3 (Degraded): The hard constraint for this state is $\rho_2 \geq d_s^a(t_k) \geq \rho_3$. For the battery, $\rho_2 = 85\%$ and $\rho_3 = 80\%$.
- State 4 (Unreliable): The hard constraint for this state is $\rho_3 \geq d_s^a(t_k)$. For the battery, $\rho_3 = 80\%$. When the

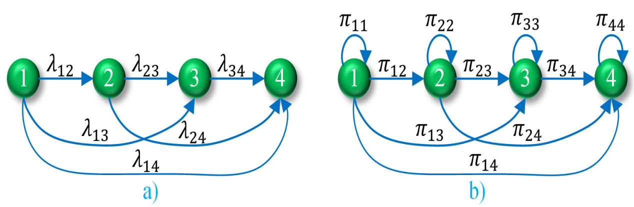

FIGURE 6. **Markov's chain degradation prediction model.**

battery reaches this state, the operation of the battery in the EV application is considered unreliable and needs to be replaced.

Modeling the degradation process of a component can be challenging due to the influence of future operating conditions in addition to the current state of the component. This study utilizes a degradation model based on Markov chain theory to address this issue. The Markov chain model considers the future operating conditions, allowing for a more accurate representation of the degradation process of the component.

Let $x_{s,i}$ denote the probability that the component s is at state $i, i \in \{1, 2, 3, 4\}$, where x_s is the vector of all $x_{s,i}$, *i.e.*, $x_s = [x_{s,1}, x_{s,2}, x_{s,3}, x_{s,4}]$. Therefore, for the Markov model depicted in Fig. 6, the transition from state x_s at time t_k to x_s at time t_{k+1} is mathematically represented by the following formula:

$$\mathbf{x_s}(t_{k+1}) = \mathbf{x_s}(t_k)\mathbf{T} \tag{5}$$

where $\mathbf{T}$ is the transition matrix

$$\mathbf{T} = \begin{bmatrix} \pi_{11} & \pi_{12} & \pi_{13} & \pi_{14} \\ \pi_{21} & \pi_{22} & \pi_{23} & \pi_{24} \\ \pi_{31} & \pi_{32} & \pi_{33} & \pi_{34} \\ \pi_{41} & \pi_{42} & \pi_{43} & \pi_{44} \end{bmatrix} \tag{6}$$

The transition matrix in the above model is now derived. Maintenance and repair are not considered in the model because the model is to aid decision makings on operation and maintenance strategies. It is typically assumed that the sojourn time in a state is the exponential distribution [46]. Denote λ_{ij} as the degradation rate from state i to state j, with $i \neq j$. It is noted that if the binary model is used, the degradation rate is the failure rate. Looking at the inflow and outflow of state i in the figure, The following equation can be obtained by looking at the inflow and outflow of state i in Fig. 6(a):

$$\frac{dx_i(t)}{dt} = -x_i(t)\sum_{j=i+1}^{4} \lambda_{ij} + \sum_{j=1}^{i-1} x_j(t)\lambda_{ji} \tag{7}$$

In (7), the term $x_i(t)\sum_{j=i+1}^{4} \lambda_{ij}$ denotes the intensity of transitioning from state i to the other states. Similarly, the term $\sum_{j=1}^{i-1} x_j(t)\lambda_{ji}$ denotes the intensity of transitioning to state i from the other states. Solving (7) and discretizing the solutions with sampling time Δt, following equations can be obtained [47].

$$\pi_{11} = e^{-(\lambda_{14}+\lambda_{13}+\lambda_{12})\Delta t} \tag{8a}$$
$$\pi_{12} = \frac{\lambda_{12}}{\lambda_{14}+\lambda_{13}+\lambda_{12}}(1 - e^{-(\lambda_{14}+\lambda_{13}+\lambda_{12})\Delta t}) \tag{8b}$$
$$\pi_{13} = \frac{\lambda_{13}}{\lambda_{14}+\lambda_{13}+\lambda_{12}}(1 - e^{-(\lambda_{14}+\lambda_{13}+\lambda_{1,2})\Delta t}) \tag{8c}$$
$$\pi_{14} = \frac{\lambda_{1,4}}{\lambda_{1,4}+\lambda_{13}+\lambda_{12}}(1 - e^{-(\lambda_{14}+\lambda_{13}+\lambda_{12})\Delta t}) \tag{8d}$$
$$\pi_{21} = 0 \tag{8e}$$
$$\pi_{22} = e^{-(\lambda_{23}+\lambda_{24})\Delta t} \tag{8f}$$
$$\pi_{23} = \frac{\lambda_{23}}{\lambda_{23}+\lambda_{24}}(1 - e^{-(\lambda_{23}+\lambda_{24})\Delta t}) \tag{8g}$$
$$\pi_{24} = \frac{\lambda_{24}}{\lambda_{23}+\lambda_{24}}(1 - e^{-(\lambda_{23}+\lambda_{24})\Delta t}) \tag{8h}$$
$$\pi_{31} = 0 \tag{8i}$$
$$\pi_{32} = 0 \tag{8j}$$
$$\pi_{33} = e^{-\lambda_{34}\Delta t} \tag{8k}$$
$$\pi_{34} = 1 - e^{-\lambda_{34}\Delta t} \tag{8l}$$
$$\pi_{41} = 0 \tag{8m}$$
$$\pi_{42} = 0 \tag{8n}$$
$$\pi_{43} = 0 \tag{8o}$$
$$\pi_{44} = 1 \tag{8p}$$

This study assumes that a component's degradation rate remains constant when the load is at or below P^{norm}. However, the degradation rate increases exponentially once the load surpasses P^{norm}. This assumption is based on the fact that the operating temperature of the component starts to rise exponentially as the load increases from this point, resulting in an exponential increase in the degradation rate [27], [48], [49]. It should be noted that the control system includes an EM and thus limits P to be less than its maximum capacity $\overline{P}$, which is one of the optimization constraints. λ_{ij} represents the degradation rate when the component operates in the range of $P < P_{norm}$, while $\underline{\lambda_{ij}}$ represents the degradation rate when the component operates at the maximum capacity $\overline{P}$. The degradation rate when the component operates between P_{norm} and $\overline{P}$ is calculated as follows.

$$\lambda_{ij} = \eta e^{\zeta P} \tag{9}$$

where

$$\zeta = \frac{\ln(\underline{\lambda_{ij}}/\overline{\lambda_{ij}})}{P^{norm} - \overline{P}} \tag{10a}$$
$$\eta = \frac{\underline{\lambda_{ij}}}{e^{\zeta P^{norm}}}. \tag{10b}$$

In order to formulate this degradation model, it becomes imperative to compute the degradation rate (λ). This rate is determined by utilizing the SNL dataset, and the algorithm for calculating the degradation rate is outlined in Section V.

2) MAXIMUM CAPACITY EXPECTATION DEGRADATION

This section introduces a mechanism for the DF layer to interact with the EM, building upon the degradation prediction methodology proposed in the previous section. The approach is to incorporate a cost factor based on the degradation results into the objective cost of the EM. To quantify the degradation of component capacity, a new parameter is introduced as follows: Let $\mathbb{P}_s(t_k)$ denote the maximum expected capacity of component s at time t_k resulting from the degradation prediction. This parameter is mathematically defined as:

$$\mathbb{P}_s(t_k) = \sum_{i=1}^{4} x_i(t_k)\overline{P_i} \tag{11}$$

The aim is to quantify the degradation of $\mathbb{P}_s(t_k)$ over a period of time. Assuming the forecast of component degradation is made from t_0 to t_k, a metric $\Delta_s(t_K)$ is presented to gauge the decline in the capacity of component s from t_0 to t_k.

$$\Delta_s(t_K) = \mathbb{P}_s(t_0) - \mathbb{P}_s(t_K) \tag{12}$$

Let ρ_s denote the cost per unit of capacity of component s at the initial time. The degradation cost is penalized by adding the following term to the objective cost of the EM.

$$f_s^d(P_s) = \rho_s \Delta_s P_s \tag{13}$$

3) RECONFIGURATION OF EM'S OPTIMIZATION PROBLEM

Section II discussed the EM and presented it in a general mathematical form in (1a). This section provides a detailed explanation of the EM's constraints and how the optimization problem is reconfigured. Typically, as discussed in Section II, the EM's optimization problem focuses mainly on fuel cost reductions. However, the degradation of electrical components becomes a problem and raises operating costs, particularly for batteries, as they account for nearly 30% of a vehicle's cost. It is challenging to determine the appropriate degradation costs. Some studies add a constant value to the total cost function, as shown in (1a), but the degradation of a component depends on its operating conditions. It is worth noting that every energy source has its generation capacity limits. Therefore, one of the constraints of (1b) is lower and upper generation limits as

$$\underline{P_{bat}} \leq P_{bat} \leq \overline{P_{bat}} \tag{14a}$$
$$\underline{P_{ICE}} \leq P_{ICE} \leq \overline{P_{ICE}} \tag{14b}$$

The main goal of powertrains is to supply loads properly. The total generation should be met the total load and any losses as shown in Fig. 7. With the considered configuration, the following constraint can be formed.

$$P_{bat} + P_{ICE} = P_{AC\ load} + P_{DC\ load} + P_{propulsion} + P_{V2X} + P_{loss} \tag{15}$$

where P_{bat} is power generated by the battery, P_{ICE} is power generated by the ICE, $P_{AC\ load}$ is AC load, $P_{DC\ load}$ is DC load, $P_{propulsion}$ is propulsion load, P_{V2X} is power used for V2X mode, and P_{loss} is the total loss.

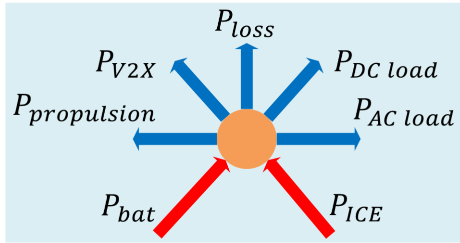

FIGURE 7. Power flow model.

Each system has its own internal constraints, i.e., (1c). The components considered in this study are ICE and battery; hence following constraints are assumed for these power-generating sources.

$$|P_{ICE}(t_{k+1}) - P_{ICE}(t_k))| < rr_{ICE} \tag{16a}$$
$$|P_{bat}(t_{k+1}) - P_{bat}(t_k)| < rr_{bat} \tag{16b}$$
$$\underline{SoC_{bat}} \leq SoC_{bat} \leq \overline{SoC_{bat}} \tag{16c}$$
$$SOC_{bat}(t_{k+1}) = SOC_{bat}(t_k) - \frac{\delta T i_{bat}}{Q_{nom}} \tag{16d}$$

where $\delta T = t_{k+1} - t_k$. Constraints (16a) and (16b) are understood both the battery and the ICE have ramp rate limits when adjusting their generation, where rr_{ICE} is the ramp rate limit for ICE and rr_{bat} is the ramp rate limit for the battery. Constraints (16c) and (16d) are the battery's State of Charge (SoC) constraints.

As previously mentioned, the EM is responsible for allocating power to the sources present in the vehicles. It determines the operating points for these units without looking into the components' degradation, shown in (9). The components' operating points (i.e., power allocation for the sources) can be adjusted by modifying the configuration of the EM's optimization problem. There are two ways to adjust the operating points of the components through EM: (a) by changing the components' maximum generation or transfer capacities and (b) by modifying the EM's objective function. In this study, adjusting the operating conditions of the components through the EM's objective function is preferred, as changing the maximum capacity of sources in the HEV is not feasible.

B. IMPLEMENTATION OF PBCF

The proposed system is graphically represented in Fig. 8, where a Markov chain model is trained and utilized to predict the component's degradation, and subsequently, the degradation cost is calculated using (9) in the degradation forecasting layer. The degradation cost is then incorporated into the EM's objective function, as shown in (17a) and (17b), through the proposed mechanism called the Prognostic-based control framework (PBCF). Once the EM's objective function is updated, it redistributes power among the sources,

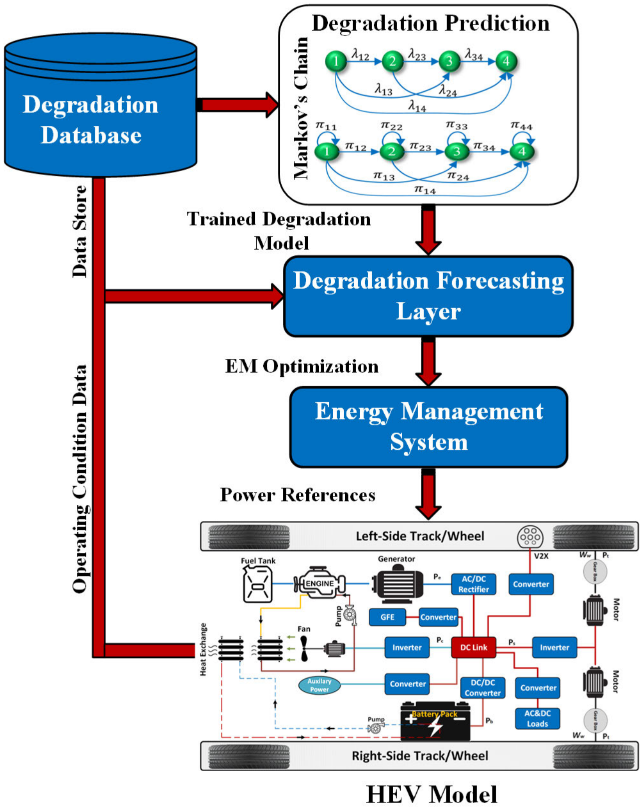

FIGURE 8. Integrating degradation forecasting into control and management system for HEVs (i.e., PBCF).

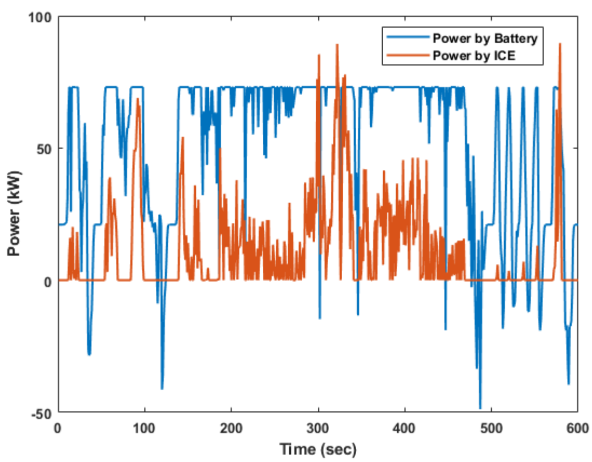

FIGURE 9. Allocation of power by EM without PBCF.

as depicted in Fig. 9 and Fig. 10.

$$\min \sum_{s \in \mathcal{S}} \left(f_s\left(P_s(t_k)\right) + f_s^d(P_s) \right) \tag{17a}$$

$$\min \sum_{s \in \mathcal{S}} \left(f_s\left(P_s(t_k)\right) + \rho_s \Delta_s P_s \right) \tag{17b}$$

Fig. 9 illustrates the power distribution between the battery and ICE, optimized using the problem statement given by (1a). As can be observed, the battery supplies most of the load demand of the powertrain, and the ICE provides power when the battery cannot meet the load requirements. This method helps to reduce fuel consumption but neglects the degradation of the battery. To account for the degradation cost given by (13), it is included in the objective function of the EM, resulting in its update as shown by (17a). This reconfiguration leads to the readjustment of power distribution between the ICE and battery, depicted in Fig. 10. With this new configuration, the ICE supplies more power to the load than in the previous case, causing less stress on the battery and minimizing degradation. Although this process increases fuel costs, the overall operational cost will be reduced, which is explained in detail with experimental results in Sections V and VI.

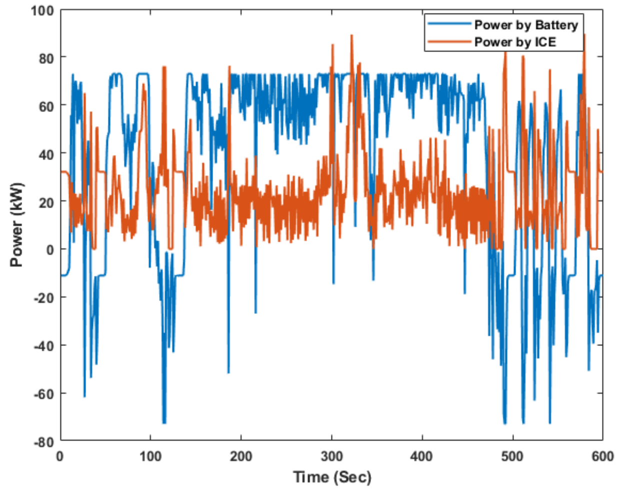

FIGURE 10. Reallocation of power by EM with the implementation of PBCF.

Fig. 9 and Fig. 10 highlight a notable increase in battery charging following the implementation of PBCF. This trend is reaffirmed by Fig. 11 after running the simulation for 100 drive cycles. This figure illustrates that prior to the introduction of PBCF, the battery's State of Charge (SoC) decreased from 80% to 60.17%. However, after implementing PBCF, the SoC decreased to 64.86%. To offer a closer examination of the SoC variations, a magnified figure representing a single drive cycle is also provided.

V. NUMERICAL SIMULATIONS

A. SYSTEM DESCRIPTION

This section uses numerical simulations to validate the proposed framework on a personal computer. The HEV powertrain, illustrated in Fig. 1 with two power sources, ICE and battery, is used for this purpose. Since this study focuses on re-configuring the objective function of EM through the proposed framework, an HEV model based on the power flow equation is developed in MATLAB/Simulink. It does not consider the system's dynamics for simplicity and reduced complexity while deploying it on MATLAB/Simulink or to a real-time simulator in Section VI. All vehicle parameters are considered from the study [36], which is then used to calculate

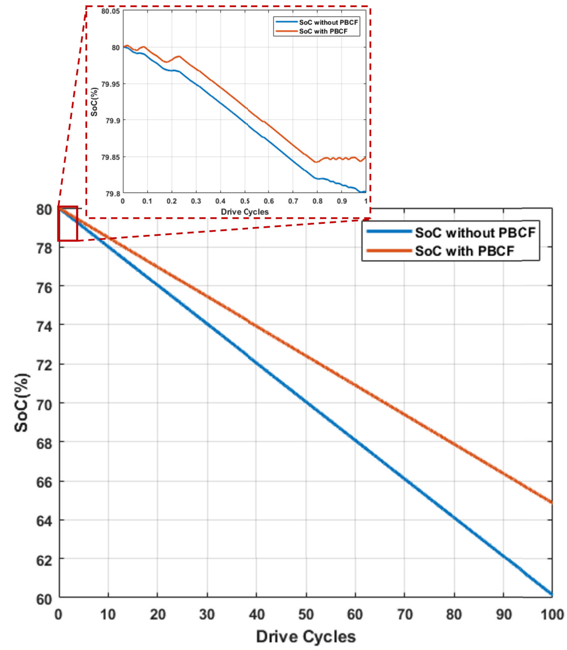

FIGURE 11. SoC of battery before and after implementing PBCF.

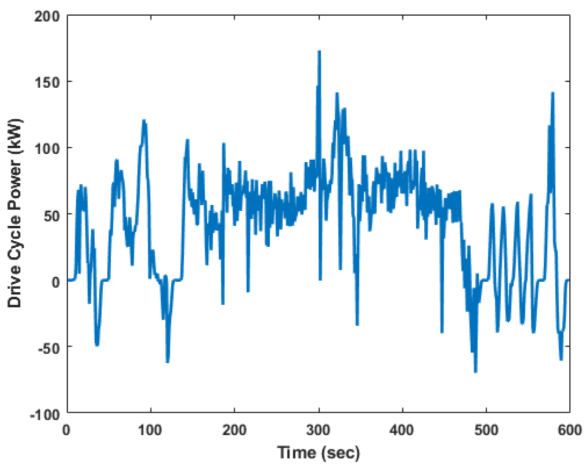

FIGURE 12. Sample of propulsion load.

the propulsion power for the US06 drive cycle using Ansys Motor-CAD. Fig. 12 illustrates a sample of the propulsion load for the US06 drive cycle used in this study, where the vehicle operates for 598 seconds and 8.01 miles in one drive cycle. The HEV's ICE capacity can generate up to 180 kW to provide the DC bus, and the battery has a capacity of 73 kWh. The propulsion load is typically the highest among the other loads when operating vehicles. In this paper, a few samples of propulsion loads are used. Additionally, throughout the simulation, the vehicle is operated in a manner that keeps the State of Charge (SoC) of the battery within predefined boundaries. These boundaries entail a minimum SoC of 40%, a maximum SoC of 90%, and the initial SoC during startup is set to 80%.

Also, the SoC of the battery is changed within certain limits, where the minimum SoC is 40%, and the maximum SoC is 90%.

B. DEGRADATION DATA

Accessing battery degradation data used in HEVs/EVs by the automotive industry is challenging since it is kept confidential. Therefore, in this study, SNL data sets are utilized, as discussed previously. The battery cell data on degradation is used to develop the degradation model, which is explained in Section IV, and then scaled up to the battery capacity used in this study. From the generated data, different degradation paths for different cells are used to obtain minimum degradation intensity matrix $\underline{\lambda} = [\lambda_{ij}]_{4\times4}$ using Algorithm 1. Algorithm 1 utilizes the array d_y to store a degradation pattern while the array S_y holds the state of all elements in d_y. Y denotes the total number of generated degradation paths. The algorithm is designed to calculate the transition probability from state i to state j. Additionally, the maximum degradation intensity matrix $\overline{\lambda} = [\lambda_{ij}]_{4\times4}$ can also be computed using this algorithm. Similarly, the Wiener process is used to model ICE degradation, as explained in detail in the previous study [27]. The same model is used in this study, with the fuel efficiency curve given by (18) where x denotes the power supplied by the ICE. The curve for this fuel efficiency is obtained from study [50]. Every model is developed and deployed in MATLAB/Simulink in this section.

$$f(x) = 0.00052\,x^2 + 0.0152\,x + 0.65 \tag{18}$$

To evaluate the economic feasibility of the proposed framework, it is essential to consider the initial costs of both the ICE and battery. According to recent reports from [51], the average cost of a Lithium-ion battery per kWh is around \$140 in 2021. Furthermore, the initial cost of the ICE is considered approximately \$7000 [5].

Algorithm 1 Training Minimum Degradation Intensity Matrix

1. Input: Degradation paths d_y, $y \in \{1, \ldots., Y\}$
2. Initialize: $\underline{\lambda} = [0]_{4\times4}$
3. **for** $y := 1$ *to* Y **do**
   Assign state for $d_y(l)$: $S_y(l) = i,\ i = 1\ or\ i = 2\ or\ i = 3\ or\ i = 4$
   for $l := 2$ *to* $length(d_y) - 1$ **do**
      Assign state for $d_y(l)$: $S_y(l) = i,\ i = 1\ or\ i = 2\ or\ i = 3\ or\ i = 4$
      $\underline{\lambda}(S_y(l-1), S_y(l)) = \underline{\lambda}(S_y)(l-1), S_y(l) + 1$
   end
   end
4. Normalize $\underline{\lambda}$
5. **return** $\underline{\lambda}$

C. NUMERICAL SIMULATION RESULTS AND DISCUSSION

The simulation was conducted to compare two cases: one without the implementation of the PBCF and another with the PBCF. In the first case, the DF layer is not utilized, while in

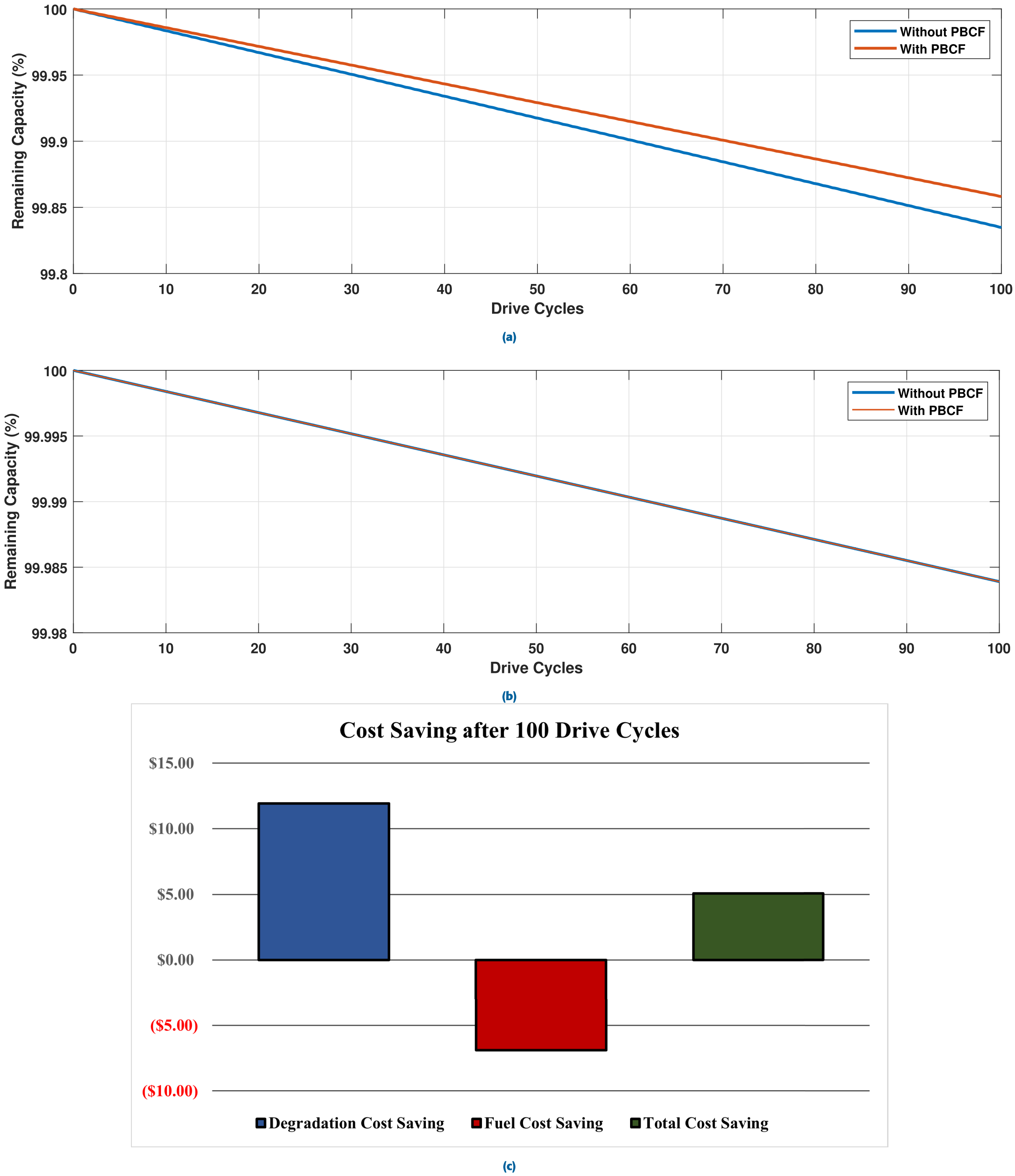

FIGURE 13. **Simulation results: (a) Battery degradation abatement (b) ICE degradation abatement (c) Cost savings by the proposed PBCF.**

the second case, the DF layer uses a Markov chain model to predict degradation. The degradation cost predicted by the DF layer is then incorporated into the objective function of the EM system.

The degradation forecasting is performed for both the battery and the ICE at a temperature of 25°C after running 100 drive cycles. The results of the simulation are presented in Fig. 13. It can be observed from Fig. 13a that the implementation of the PBCF strategy leads to a reduction in the battery degradation path. However, as seen from Fig. 13b there is no significant change in the degradation path of the ICE, as the simulation is only run for 100 drive cycles, and the degradation of the ICE is relatively lower compared to the battery. Because of this reason, the degradation path of ICE is not observed in real-time simulation.

Fig. 13c demonstrates that the PBCF strategy effectively reduces the degradation costs of the battery and the ICE by $11.94. However, it is important to note that there is an increase in fuel cost of $6.879 due to the higher power supplied by the ICE, as shown in Fig. 10. Overall, the PBCF strategy results in a net reduction of \$5.066 in operating costs after 100 drive cycles. Additionally, the PBCF strategy successfully mitigates battery degradation.

VI. CHIL EXPERIMENT

The implementation of the proposed strategy is demonstrated through a CHIL experiment conducted on a series HEV system, as explained in Section III. The equipment from Clemson University's Real-time Control and Optimization Laboratory (RT-COOL) is used to integrate the DF layer with the EM to develop the PBCF approach. The objective of a CHIL experiment utilizing laboratory equipment is to demonstrate the viability of implementing the proposed framework in application in real-time and its efficient integration with the other additional layers along with the EM. The subsequent section presents further information on the CHIL implementation and the experimental outcomes.

A. SYSTEM MODELING

The series HEV is simulated in the schematic editor in Typhoon HIL control center software. The schematic editor develops the HEV model based on the power flow equation between the sources and loads. This model is then compiled and loaded into HIL SCADA, which is then deployed into the real-time digital simulator (RTDS) Typhoon HIL 606. In Section III, a model is developed using the power flow equation instead of developing a comprehensive dynamic model of the vehicle. The same model is deployed here in Typhoon because this study focuses not on examining the vehicle's dynamics but on developing control on allocating power for multiple sources to fulfill the vehicle's load demand. This approach simplifies the model's complexity in contrast to utilizing the complete dynamic model of the vehicle.

To manage multiple power sources in a vehicle, an EM is necessary, as discussed in Section II. In the automotive industry, EM algorithms are typically deployed in a controller called Electronic Control Units (ECUs). Here, a Raspberry Pi 4 Model B is used as the ECU to run the EM algorithm, which aims to reduce fuel cost, as described in Section II. The real operating parameters from the HEV model (i.e., Typhoon) are sent to the Raspberry Pi, which runs the EM algorithm to determine the optimal reference power to be supplied by the battery and ICE. This reference power is then sent back to the Typhoon.

The EM employs three threads running in parallel (utilizing three out of the four cores of the Raspberry Pi). The first thread waits for the signal (whether the system has started or not) to begin the EM algorithm, while the second thread handles communication protocol, receiving the battery's SoC and all the loads demanded by the vehicle. Finally, the third thread runs the EM algorithm and returns the reference power back to Typhoon using the communication protocol deployed in the second thread. The standard communication protocol used in the vehicles is Controller Area Network (CAN) communication. Therefore, in this project, CAN communication transfers the data between the simulator and the ECUs. Fig. 14 illustrates the implementation of the proposed strategy in real-time through a CHIL setup.

B. COMMUNICATION

Controller Area Network (CAN) is a widely used communication protocol for transferring data in automotive and industrial applications. In a CAN network, data is transferred between different electronic control units (ECUs), also known as nodes, through two wires named CAN HIGH (CAN-H) and CAN LOW (CAN-L).

All the nodes are connected to the CAN bus, and when a node wants to transmit data, it checks the bus to ensure it is idle. If the bus is free, the node begins transmitting its message by placing it on the bus. Each node on the network receives the message and checks the identifier. Here each message consists of an identifier, which specifies the priority and content of the message and the data to be transferred. In this study, there are three nodes as follows:

- Typhoon (HEV Model)
- Raspberry Pi (ECU-1, EM)
- Raspberry Pi (ECU-2, DF)

Data transmission in a CAN involves disseminating data from one node to the CAN bus, which can be accessed by all other nodes in the network. In this study, Typhoon uses its own interface to establish a CAN network, employing CAN send and CAN receive blocks for data transmission. For targeted communication, a designated message-id is assigned to transmit data to specific ECUs such as ECU-1 (EM) and ECU-2 (DF). On the receiving end, the message-id is verified to ensure that the respective ECU receives the intended data. Similarly, in Raspberry Pis, Python code facilitates data exchange through the CAN bus. This approach enables each node to transmit and receive signals using specific message ids, ensuring reliable communication while mitigating interference. The establishment of CAN communication in RT-COOL is illustrated in Fig. 15.

C. INTEGRATING DEGRADATION FORECASTING INTO THE EM

The previous section explains the EM's approach, which aims to minimize fuel costs and allocate power across each source used in the vehicle. The EM, however, won't evaluate the degradation of the components, which may increase the vehicle's overall running costs. The DF layer is integrated above the EM for this reason. Now, the reference powers generated by the EM are fed into the HEV model and also to the DF layer to predict the degradation of the components using CAN communication.

The proposed DF algorithm is developed using the Python environment and is deployed in a real-time ECU, the Raspberry Pi 4 Model B. This ECU receives signals from another ECU that hosts the EM and RTDS, where the HEV model is deployed. Depending on the signals received, the ECU predicts the degradation rate using the developed Markov chain model, as explained in Section IV-A1. The trained

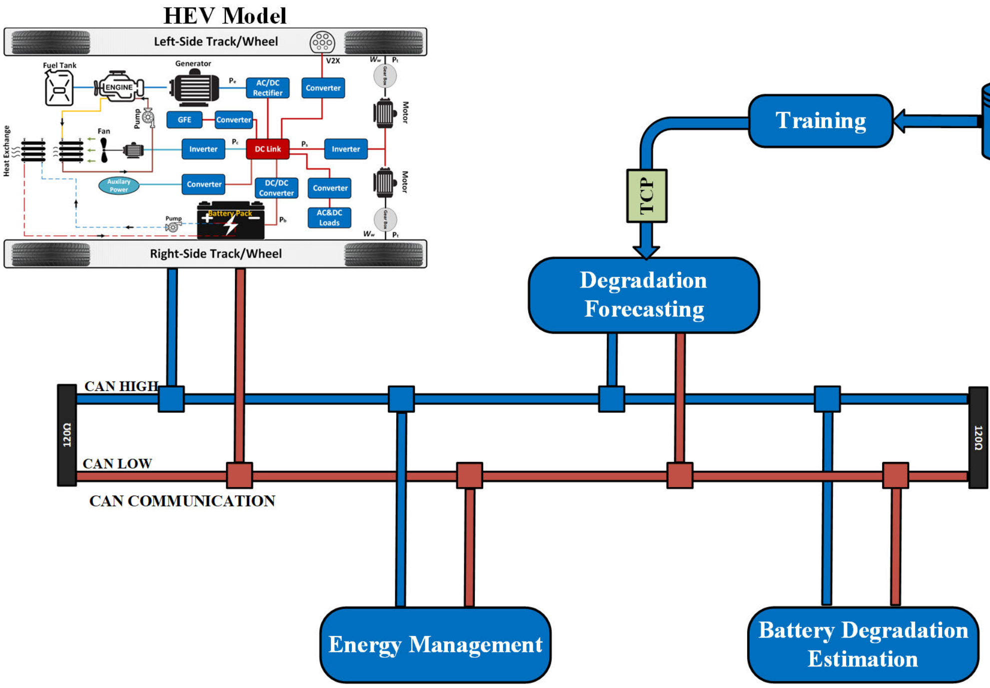

FIGURE 14. CHIL implementation for real-time PBCF.

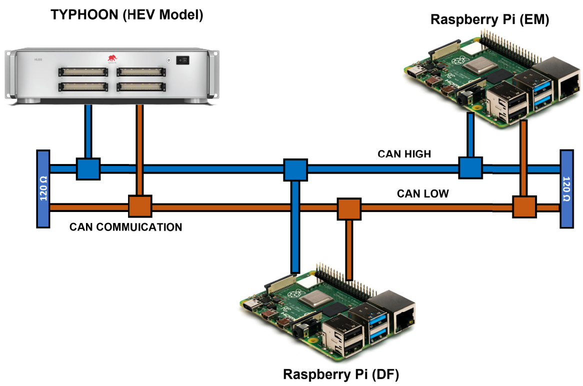

FIGURE 15. CHIL implementation of PBCF in real-time on actual components in RT-COOL.

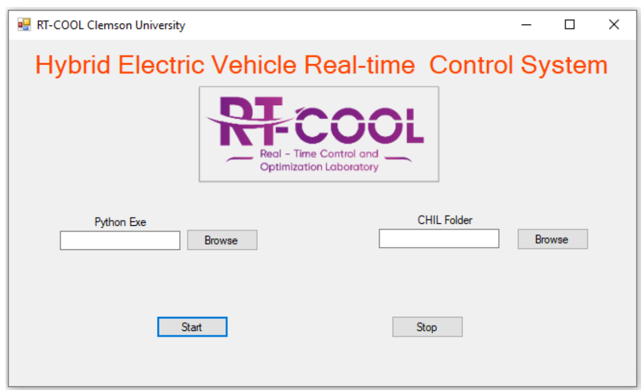

FIGURE 16. Real-Time implementation control screen.

Markov chain model is obtained from a computer acting as a server, with its functionalities implemented using a Python script. The server's functionalities involve storing and training data using Algorithm 1 to obtain each information source's maximum and minimum degradation intensity matrices. Additionally, it sends trained models whenever the real-time controller that implements the DF requests them and stores the necessary scripts for the EM and DF in their respective controllers. Finally, the DF controller collaborates with the server to run the Markov chain degradation model presented in Section IV-A1 and predict the components' degradation rate.

The degradation cost is estimated using (13), based on the degradation rate and the capacity lost over time. This cost is then transmitted to the EM, which incorporates it as a penalized degradation cost in its objective function and adjusts the power allocation between the sources accordingly. The communication between the ECUs and the RTDS is facilitated through CAN communication, as explained in Section VI-B.

An interface is included for monitoring the system, called the human-machine interface (HMI). A HIL SCADA window from the Typhoon control center and Python visualization environment are set up to fulfill this function. The Typhoon gathers operating data from the simulator and all ECUs, including the EM and DF controllers, and displays them on the SCADA window. The HMI includes four primary screens: the control screen, HEV monitoring screen, energy management screen, and degradation forecasting screen. The control screen has start/stop buttons and inputs for CHIL system information,

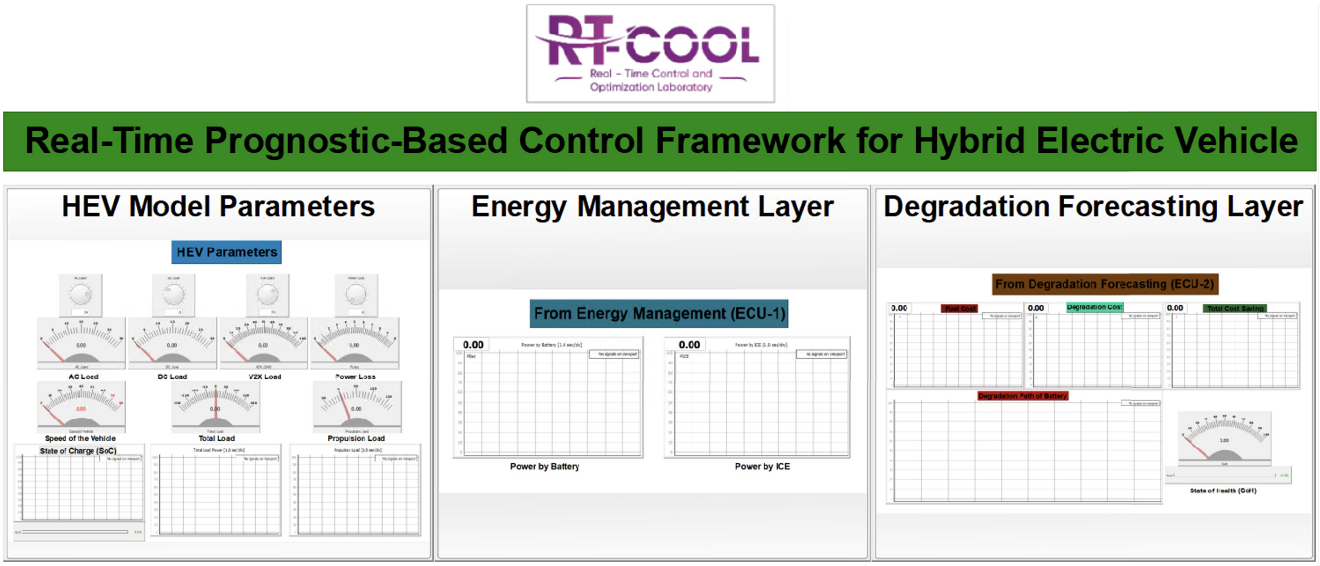

FIGURE 17. Visualization screen from CHIL experiment in SCADA window in Typhoon control center.

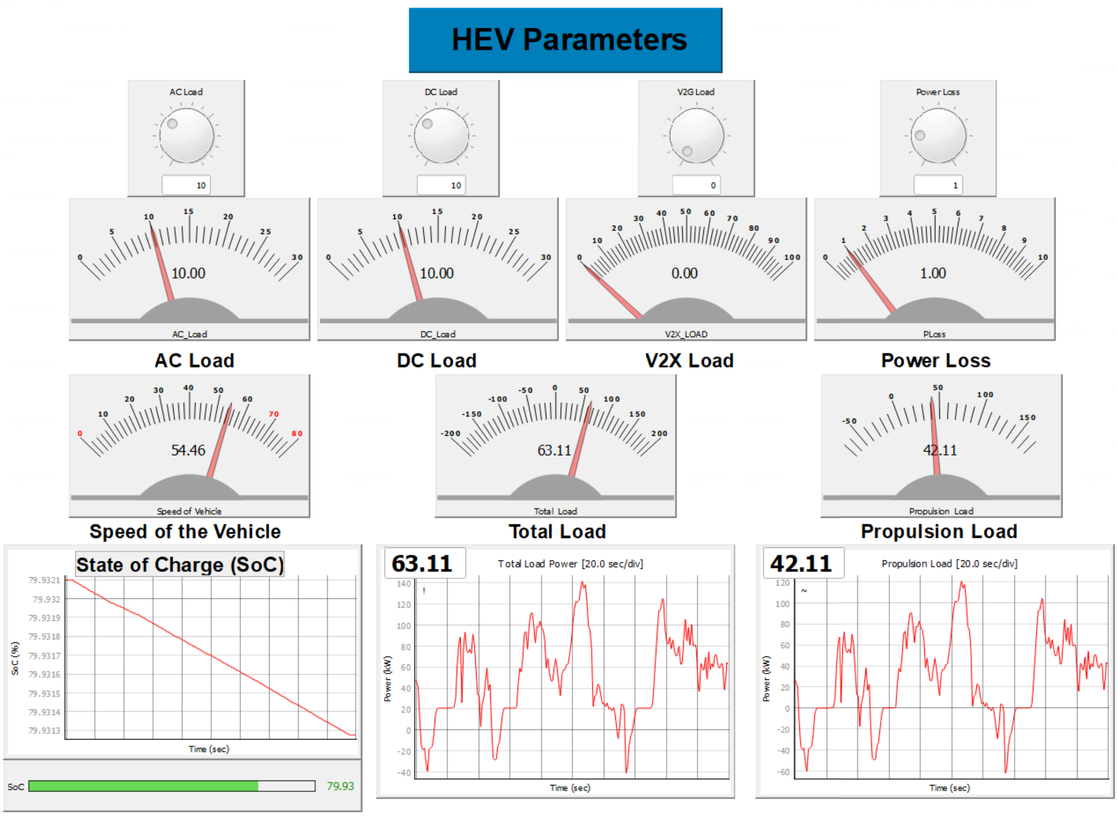

FIGURE 18. HMI display for HEV model parameters in real-time.

such as IP addresses for all the controllers (ECUs), simulators, and the host PC. The HEV monitoring screen displays all the loads demanded by the series HEV, the vehicle's speed, and the SoC of the battery used in the vehicle. The vehicle is modeled so that the users can control all the loads in real-time when the system is running, except the propulsion load, since the vehicle is driven using a predefined drive cycle. The energy management screen shows the data transmitted by the EM controller to the Typhoon, which displays the power allocated by the EM to the battery and ICE to match the power demanded by the vehicle. Lastly, the degradation forecasting screen shows the battery's degradation path and its remaining

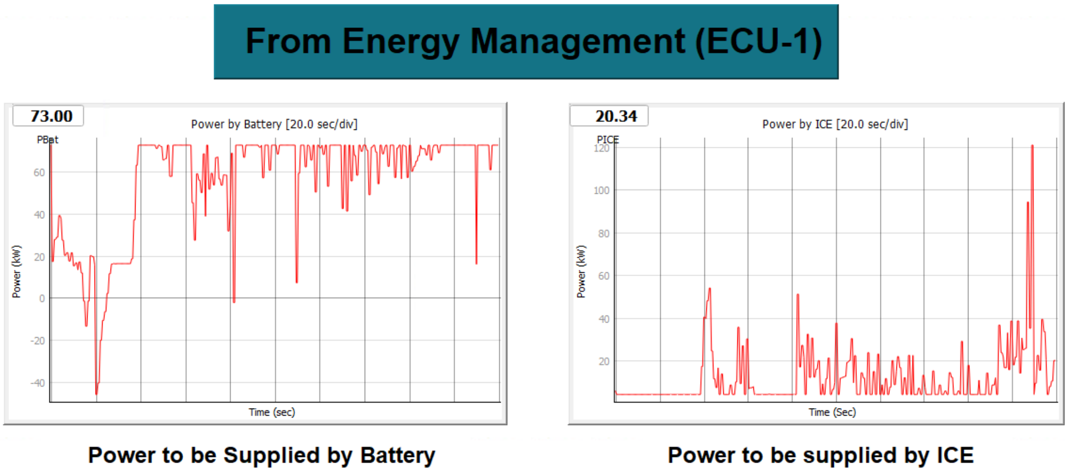

FIGURE 19. HMI display for EM layer in real-time.

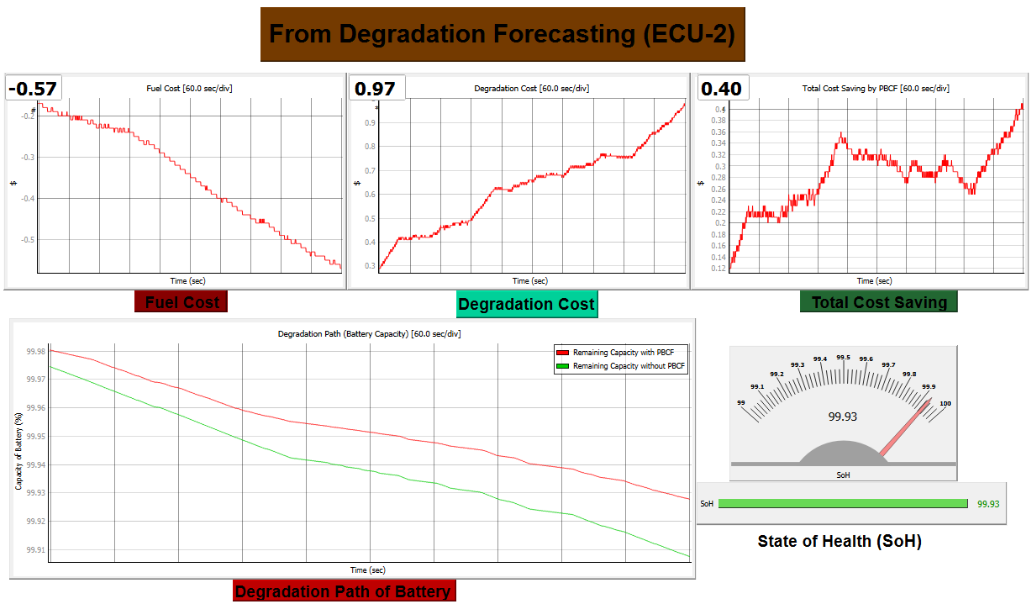

FIGURE 20. HMI display for DF layer in real-time.

capacity, also known as state-of-health (SoH), received from the DF controller. It also displays the degradation rate cost, fuel cost, and total savings achieved through the proposed control strategy. Fig. 16 displays the main control implementation screen; after pressing the start button, the CHIL experiment will start to operate. Before pressing the start button, the Python executable file must be selected as all the codes are written in Python, and the directory that has all the codes to run this project must be selected in the CHIL folder shown in the figure. Fig. 17 displays the main monitoring screen, which has three subsections: HEV monitoring, Energy Management layer, and Degradation Forecasting Layer. Each subsection shows the result from different controllers. Fig. 18 displays the parameters of an HEV considered in this project. Fig. 19 shows the optimized results sent from the EM layer to the Typhoon, whereas Fig. 20 presents the result from the DF layer. As previously mentioned, all data exchange between the ECUs and the RTDS is conducted using CAN communication.

D. EXPERIMENTAL RESULTS

The constructed CHIL system described in Fig. 14 and Fig. 15 is run, and the two layers, EM and DF, along with the HEV model, work synergically. Fig. 19, shows that the proposed EM is running in real-time, and the ECU sends the data to Typhoon with the reference powers to be supplied by the ICE and battery to drive the power-train. Also, in Fig. 20, remaining capacity of the battery along with the cost savings are sent from the DF controller to HMI running in the Typhoon for displaying. The figure displays a screenshot taken after 80 minutes, which is approximately equal to 8 drive cycles. After running for this duration, the application of PBCF resulted in a fuel cost increase of \$0.57, while the degradation cost was reduced by \$0.97. Thus, the total cost saving amounted to \$0.4. Now, repeating the same US06 drive cycle and scaling it to 100 drive cycles, the fuel cost would increase by \$7.125, while the degradation cost would decrease by \$12.12, and the total cost saving would be \$4.995. These results closely align with the MATLAB/Simulink simulation results in Section V. Additionally, the degradation path plot clearly illustrates that the application of PBCF minimizes battery degradation.

VII. CONCLUSION AND FUTURE WORK

This paper proposes a prognostic-based control framework (PBCF) where a degradation forecasting layer is integrated as an upper layer to the vehicle's energy management to minimize the degradation processes of a battery to reduce the overall operating costs. A Markov chain-based degradation model is constructed to predict the degradation paths of HEVs components in which components' states are modeled by a multi-state model. The battery data from Sandia National Laboratory is used to train Markov's degradation prediction model. The predicted results are used to adjust EM, a PBCF concept component, to abate the degradation of the battery when it has a higher degradation rate cost. The proposed strategy is verified on a series HEV model by numerical simulations done in MATLAB/Simulink. In addition, CHIL experimentation for the proposed scheme is implemented with laboratory equipment. Both numerical simulations and CHIL experimentation show operation cost savings for the studied system and the abatement of degradation for the battery.

There are research directions that can extend this work, for example:

- First, the proposed framework can be applied to other types of electric vehicles (EVs) by changing the algorithm of the EM as per the vehicle types considered
- Second, investigating the impact of V2X connection on the batteries of EVs or HEVs could be a future research direction for this work
- Third, the proposed framework can be used to investigate degradation forecasting of multiple components like power electronics devices, motors, and generators used in a vehicle and analyze the overall impact.

ACKNOWLEDGMENT

This work was supported by Clemson University's Virtual Prototyping of Autonomy Enabled Ground Systems (VIPR-GS) under Cooperative Agreement W56HZV-21-2-0001 with the US Army DEVCOM Ground Vehicle Systems Center (GVSC).

DISTRIBUTION STATEMENT A. Approved for public release; distribution is unlimited (OPSEC 7601).

REFERENCES

[1] A. Moghassemi, D. S. Vanaja, J. Olamaei, G. Ozkan, and C. S. Edrington, "A novel switching method in PV-fed quasi-ZSI-DVR for voltage quality enhancement of photovoltaic integrated networks," *IET Renew. Power Gener.*, pp. 1–20, 2022, doi: 10.1049/rpg2.12575.

[2] C.-N. Wang, F.-C. Yang, N. T. M. Vo, and V. T. T. Nguyen, "Enhancing lithium-ion battery manufacturing efficiency: A comparative analysis using DEA Malmquist and epsilon-based measures," *Batteries*, vol. 9, no. 6, p. 317, Jun. 2023.

[3] F. Ju, N. Murgovski, W. Zhuang, X. Hu, Z. Song, and L. Wang, "Predictive energy management with engine switching control for hybrid electric vehicle via ADMM," *Energy*, vol. 263, Jan. 2023, Art. no. 125971.

[4] A. Moghassemi, S. Padmanaban, V. K. Ramachandaramurthy, M. Mitolo, and M. Benbouzid, "A novel solar photovoltaic fed TransZSI-DVR for power quality improvement of grid-connected PV systems," *IEEE Access*, vol. 9, pp. 7263–7279, 2021.

[5] P. H. Hoang, G. Ozkan, P. Badr, L. Timilsina, and C. Edrington, "A prognostic based control framework for hybrid electric vehicles," SAE, Tech. Paper 2022-01-0352, 2022, doi: 10.4271/2022-01-0352.

[6] E. Buraimoh, G. Ozkan, L. Timilsina, P. K. Chamarthi, B. Papari, and C. S. Edrington, "Overview of interface algorithms, interface signals, communication and delay in real-time co-simulation of distributed power systems," *IEEE Access*, vol. 11, pp. 103925–103955, 2023.

[7] S. M. I. Rahman, M. R. Hazari, S. U. Hani, B. B. Pathik, M. A. Mannan, A. Mahfuz, M. K. Alam, and M. K. Hassan, "Primary frequency control of large-scale PV-connected multi-machine power system using battery energy storage system," *Int. J. Power Electron. Drive Syst.*, vol. 12, no. 3, p. 1862, Sep. 2021.

[8] Bloomberg. (2020). *Batteries for Electric Cars Speed Toward a Tipping Point*. vol. 134. [Online]. Available: http://bloomberg.com

[9] S. F. Tie and C. W. Tan, "A review of energy sources and energy management system in electric vehicles," *Renew. Sustain. Energy Rev.*, vol. 20, pp. 82–102, Apr. 2013, doi: 10.1016/J.RSER.2012.11.077.

[10] A. Sciarretta, "A control benchmark on the energy management of a plug-in hybrid electric vehicle," *Control Eng. Pract.*, vol. 29, pp. 287–298, Aug. 2014.

[11] L. Serrao, S. Onori, and G. Rizzoni, "A comparative analysis of energy management strategies for hybrid electric vehicles," *J. Dyn. Syst., Meas., Control*, vol. 133, no. 3, May 2011, Art. no. 031012.

[12] E. Silvas, T. Hofman, N. Murgovski, L. F. P. Etman, and M. Steinbuch, "Review of optimization strategies for system-level design in hybrid electric vehicles," *IEEE Trans. Veh. Technol.*, vol. 66, no. 1, pp. 57–70, Jan. 2017.

[13] D. Bianchi, L. Rolando, L. Serrao, S. Onori, G. Rizzoni, N. Al-Khayat, T.-M. Hsieh, and P. Kang, "A rule-based strategy for a series/parallel hybrid electric vehicle: An approach based on dynamic programming," in *Proc. Dyn. Syst. Control Conf.*, vol. 44175, 2010, pp. 507–514.

[14] J. Li, H. He, Z. Wei, and X. Zhang, "Hierarchical sizing and power distribution strategy for hybrid energy storage system," *Automot. Innov.*, vol. 4, no. 4, pp. 440–447, Nov. 2021.

[15] L. Tang, G. Rizzoni, and S. Onori, "Energy management strategy for HEVs including battery life optimization," *IEEE Trans. Transport. Electrific.*, vol. 1, no. 3, pp. 211–222, Oct. 2015.

[16] S. Onori, P. Spagnol, V. Marano, Y. Guezennec, and G. Rizzoni, "A new life estimation method for lithium-ion batteries in plug-in hybrid electric vehicles applications," *Int. J. Power Electron.*, vol. 4, no. 3, pp. 302–312, 2012.

[17] E. Buraimoh, G. Ozkan, L. Timilsina, A. Arsalan, B. Papari, P. K. Chamarthi, and C. Edrington, "Model free time delay compensation for damped impedance method interfaced power system co-simulation testing," SAE, Tech. Paper 2023-01-1600, 2023, doi: 10.4271/2023-01-1600.

[18] C. Zhu, F. Lu, H. Zhang, J. Sun, and C. C. Mi, "A real-time battery thermal management strategy for connected and automated hybrid electric vehicles (CAHEVs) based on iterative dynamic programming," *IEEE Trans. Veh. Technol.*, vol. 67, no. 9, pp. 8077–8084, Sep. 2018.

[19] O. Ciftci, M. Mehrtash, and A. Kargarian, "Data-driven nonparametric chance-constrained optimization for microgrid energy management," *IEEE Trans. Ind. Informat.*, vol. 16, no. 4, pp. 2447–2457, Apr. 2020.

[20] P. H. Hoang, G. Ozkan, P. R. Badr, B. Papari, C. S. Edrington, M. A. Zehir, B. Hayes, L. Mehigan, D. A. Kez, and A. M. Foley, "A dual distributed optimal energy management method for distribution grids with electric vehicles," *IEEE Trans. Intell. Transp. Syst.*, vol. 23, no. 8, pp. 13666–13677, Aug. 2022.

[21] G. Suri and S. Onori, "A control-oriented cycle-life model for hybrid electric vehicle lithium-ion batteries," *Energy*, vol. 96, pp. 644–653, Feb. 2016.

[22] L. Timilsina, P. R. Badr, P. H. Hoang, G. Ozkan, B. Papari, and C. S. Edrington, "Battery degradation in electric and hybrid electric vehicles: A survey study," *IEEE Access*, vol. 11, pp. 42431–42462, 2023.

[23] Z. Song, H. Hofmann, J. Li, J. Hou, X. Han, and M. Ouyang, "Energy management strategies comparison for electric vehicles with hybrid energy storage system," *Appl. Energy*, vol. 134, pp. 321–331, Dec. 2014, doi: 10.1016/J.APENERGY.2014.08.035.
[24] N. Sapkota, S. Chiluwal, P. Parajuli, A. Rowland, and R. Podila, "Insights into the pseudocapacitive behavior of sulfurized polymer electrodes for Li–S batteries," *Adv. Sci.*, vol. 10, no. 15, 2023, Art. no. 2206901.
[25] Z. Shi, H. Liang, S. Huang, and V. Dinavahi, "Distributionally robust chance-constrained energy management for islanded microgrids," *IEEE Trans. Smart Grid*, vol. 10, no. 2, pp. 2234–2244, Mar. 2019.
[26] A. Cuneo, V. Zaccaria, D. Tucker, and A. Traverso, "Probabilistic analysis of a fuel cell degradation model for solid oxide fuel cell and gas turbine hybrid systems," *Energy*, vol. 141, pp. 2277–2287, Dec. 2017.
[27] P. H. Hoang, G. Ozkan, P. R. Badr, L. Timilsina, B. Papari, and C. S. Edrington, "Integrating degradation forecasting into distribution grids' advanced distribution management systems," *Int. J. Electr. Power Energy Syst.*, vol. 150, Aug. 2023, Art. no. 109071.
[28] J. Du, X. Zhang, T. Wang, Z. Song, X. Yang, H. Wang, M. Ouyang, and X. Wu, "Battery degradation minimization oriented energy management strategy for plug-in hybrid electric bus with multi-energy storage system," *Energy*, vol. 165, pp. 153–163, Dec. 2018.
[29] N. Guo, X. Zhang, Y. Zou, L. Guo, and G. Du, "Real-time predictive energy management of plug-in hybrid electric vehicles for coordination of fuel economy and battery degradation," *Energy*, vol. 214, Jan. 2021, Art. no. 119070.
[30] G. dos Reis, C. Strange, M. Yadav, and S. Li, "Lithium-ion battery data and where to find it," *Energy AI*, vol. 5, Sep. 2021, Art. no. 100081.
[31] G. Muriithi and S. Chowdhury, "Optimal energy management of a grid-tied solar PV-battery microgrid: A reinforcement learning approach," *Energies*, vol. 14, no. 9, p. 2700, May 2021.
[32] A. Tang, Y. Jiang, Q. Yu, and Z. Zhang, "A hybrid neural network model with attention mechanism for state of health estimation of lithium-ion batteries," *J. Energy Storage*, vol. 68, Sep. 2023, Art. no. 107734.
[33] SN Lab. *Data for Degradation of Commercial Lithium-Ion Cells as a Function of Chemistry and Cycling Conditions*. Accessed: Jun. 11, 2022. [Online]. Available: https://www.batteryarchive.org/snl_study.html
[34] L. Timilsina, P. H. Hoang, A. Arsalan, G. Ozkan, B. Papari, and C. S. Edrington, "Degradation abatement in hybrid electric vehicles using data-driven technique," *Transp. Res. Proc.*, vol. 70, pp. 52–60, 2023.
[35] W. Zhuang, S. L. Eben, X. Zhang, D. Kum, Z. Song, G. Yin, and F. Ju, "A survey of powertrain configuration studies on hybrid electric vehicles," *Appl. Energy*, vol. 262, Mar. 2020, Art. no. 114553.
[36] Q. Zhu, A. Kumar, A. Sundar, D. Egan, H. Mirzaei, D. Chang, M. Schmid, R. Prucka, B. Lawler, and C. Paredis, "Development of a series hybrid electrified powertrain for a high speed tracked vehicle based on driving cycle simulation," *SAE Int. J. Adv. Current Practices Mobility*, vol. 4, no. 4, pp. 1403–1412, Mar. 2022.
[37] S. Onori, L. Serrao, and G. Rizzoni, *Hybrid Electric Vehicles: Energy Management Strategies*. New York, NY, USA: Springer, 2016, doi: 10.1007/978-1-4471-6781-5.
[38] P. K. Chamarthi, C. Edrington, A. Arsalan, L. Timilsina, B. Papari, G. Ozkan, and A. Moghassemi, "A novel 1-ϕ cuk based on-board electric vehicle charger with minimal number of power components," SAE, Tech. Paper 2023-01-1686, 2023, doi: 10.4271/2023-01-1686.
[39] A. Arsalan, L. Timilsina, B. Papari, G. Muriithi, G. Ozkan, P. Kumar, and C. S. Edrington, "Cyber attack detection and classification for integrated on board electric vehicle chargers subject to stochastic charging coordination," *Transp. Res. Proc.*, vol. 70, pp. 44–51, 2023.
[40] S. M. Sabet, N. Sapkota, S. Chiluwal, T. Zheng, C. M. Clemons, A. M. Rao, and S. Pilla, "Sulfurized polyacrylonitrile impregnated delignified wood-based 3D carbon framework for high-performance lithium–sulfur batteries," *ACS Sustain. Chem. Eng.*, vol. 11, no. 6, pp. 2314–2323, 2023.
[41] E. Gumrukcu, A. Arsalan, G. Muriithi, C. Joglekar, A. Aboulebdeh, M. Alparslan Zehir, B. Papari, and A. Monti, "Impact of cyber-attacks on EV charging coordination: The case of single point of failure," in *Proc. 4th Global Power, Energy Commun. Conf. (GPECOM)*, Jun. 2022, pp. 506–511.
[42] Z. Deng, L. Xu, H. Liu, X. Hu, Z. Duan, and Y. Xu, "Prognostics of battery capacity based on charging data and data-driven methods for on-road vehicles," *Appl. Energy*, vol. 339, Jun. 2023, Art. no. 120954.
[43] Z. Li, T. Xu, J. Gu, Q. Dong, and L. Fu, "Reliability modelling and analysis of a multi-state element based on a dynamic Bayesian network," *Roy. Soc. Open Sci.*, vol. 5, no. 4, Apr. 2018, Art. no. 171438.
[44] Q. T. Tu Tran, K. Davies, L. Roose, B. V. Doan, and N. Q. Nguyen, "Online distribution service transformer health assessment using real-time grid energy monitor," in *Proc. IEEE Kansas Power Energy Conf. (KPEC)*, Jul. 2020, pp. 1–6.
[45] E. Möllerström, F. Ottermo, A. Goude, S. Eriksson, J. Hylander, and H. Bernhoff, "Turbulence influence on wind energy extraction for a medium size vertical axis wind turbine," *Wind Energy*, vol. 19, no. 11, pp. 1963–1973, Nov. 2016.
[46] R. Billinton and R. N. Allan, *Reliability Evaluation of Power Systems*, 2nd ed. New York, NY, USA: Plenum Press, 1996.
[47] P. H. Hoang, P. R. Badr, G. Ozkan, C. S. Edrington, and B. Papari, "Integrating degradation forecasting into control and management system of DC microgrids," in *Proc. IEEE 4th Int. Conf. DC Microgrids (ICDCM)*, Jul. 2021, pp. 1–6.
[48] N. Mo, Z. Y. Zou, K. W. Chan, and T. Y. G. Pong, "Transient stability constrained optimal power flow using particle swarm optimisation," *IET Gener., Transmiss. Distribution*, vol. 1, no. 3, p. 476, 2007.
[49] A. M. Emsley and G. C. Stevens, "Review of chemical indicators of degradation of cellulosic electrical paper insulation in oil-filled transformers," *IEE Proc. Sci., Meas. Technol.*, vol. 141, no. 5, pp. 324–334, Sep. 1994.
[50] P. H. Hoang, G. Ozkan, P. R. Badr, B. Papari, and C. S. Edrington, "Distributed constrained optimization by singular perturbation method and its application to energy networks by real-time implementation," *Sustain. Energy, Grids Netw.*, vol. 27, Sep. 2021, Art. no. 100473.
[51] The Economist. (2021). *Lithium Battery Costs Have Fallen by 98% in Three Decades*. vol. 134. [Online]. Available: http://https://www.economist.com/

LAXMAN TIMILSINA (Graduate Student Member, IEEE) received the B.E. degree in electrical engineering from the Institute of Engineering, Tribhuvan University, Nepal, in 2016, the M.Sc. degree in distributed generation and in electrical engineering from Tribhuvan University, in 2019, and the Ph.D. degree in electrical engineering from Clemson University, in Fall 2021, under the supervision of Dr. Chris S. Edrington. He is currently a Graduate Research Assistant with the Real-Time COntrol and Optimization Laboratory (RT-COOL), Holcombe Department of Electrical and Computer Engineering (ECE), Clemson University. His research interests include electric vehicles, integration of renewable energy, and smartgrids.

PHUONG H. HOANG (Member, IEEE) received the B.S. degree in control and automation engineering from the Hanoi University of Science and Technology, Vietnam, the M.S. degree in mechanical engineering from the Gwangju Institute of Science and Technology, South Korea, and the Ph.D. degree in electrical engineering from Clemson University. He is currently with the Optimization & AI Department-Research and Development Team, Operation Technology Inc. (ETAP)-USA (A Schneider Electric Subsidiary). His research interests include optimization for power systems, degradation forecasting, and machine learning.

ALI MOGHASSEMI (Graduate Student Member, IEEE) received the B.S. and M.S. degrees in electrical engineering from Islamic Azad University, South Tehran Branch, Tehran, Iran, in 2012 and 2015, respectively, and the Ph.D. degree in electrical engineering from Clemson University, Clemson, USA, in Fall 2022, under the supervision of Dr. Christopher S. Edrington. He is currently a Graduate Research Assistant with RT-COOL, Holcombe Department of Electrical and Computer Engineering, Clemson University. His research interests include modeling, simulation, and real-time modeling of power electronics and renewable energy systems. Plus, he has been serving as a reviewer for several scientific journals over the years.

ELUTUNJI BURAIMOH (Member, IEEE) received the B.Tech. (Hons.) degree in electronic and electrical engineering from the Ladoke Akintola University of Technology, Nigeria, in 2012, the M.Sc. degree in electronic and electrical engineering from Obafemi Awolowo University, Nigeria, in 2016, and the D.Eng. degree from the Durban University of Technology, South Africa, in 2021. He is currently pursuing the Ph.D. degree with the Holcombe Department of Electrical and Computer Engineering, Clemson University. He is a Research Assistant with the Virtual Prototyping of Autonomy-Enabled Ground Systems (VIPR-GS) Centre, Clemson University. His research interests include geographically distributed real-time co simulation of power systems, military-based vehicle-to-grid and vehicle-to-vehicle microgrids, advanced power management, reinforcement learning, and energy management. He is a registered Engineer of the COREN, a Corporate Member of the NSE, a Candidate for ECSA, and a member of SAE.

PHANI KUMAR CHAMARTHI (Member, IEEE) received the combined M.Tech. and Ph.D. degrees in power electronics and power systems from the Department of Electrical and Electronics Engineering, Indian Institute of Technology Bombay, Mumbai, India, in 2018. He is currently a Postdoctoral Fellow with Clemson University, USA. His research interests include new single-stage transformerless inverter topologies, multilevel converter topologies, space vector control of multilevel converters, and new modulation and control strategies of multilevel converters, focusing on renewable energy applications.

GOKHAN OZKAN (Senior Member, IEEE) received the B.Sc. degree from the Electric Education Department, Marmara University, in 2006, the B.Sc. (as a valedictorian) and M.Sc. degrees from the Energy System Engineering Department, Erciyes University, in 2014 and 2016, respectively, and the Ph.D. degree from the Electrical and Computer Engineering Department, Florida State University, in 2019. He joined Clemson University as a Postdoctoral Fellow, in 2020. He has been a Research Assistant Professor with the Holcombe Department of Electrical and Computer Engineering, since 2021. He is currently the Research Lead of the Energy Innovation Center, North Charleston, and also the Manager of the Real-Time COntrol and Optimization Laboratory (RT-COOL). His main research interests include power systems and DER integration, model predictive control in power converters and drives, active thermal management and fault-tolerant control, distributed controls, power and EM, real-time power distribution system modeling, simulation, co-simulations, and hardware-in-the-loop instantiation.

BEHNAZ PAPARI (Senior Member, IEEE) received the B.S. degree in electrical engineering from the University of Bushehr, in 2008, the M.Sc. degree in electrical engineering from the K. N. Toosi University of Technology, Iran, in 2011, and the Ph.D. degree in electrical and computer engineering from Florida State University, USA, in 2018. Prior to joining the Department of Automotive Engineering and Electrical and Computer Engineering, Clemson University, in Spring 2022. She was an Assistant Professor with the Department of Marine Engineering Technology, Texas A&M University, and an Assistant Professor in practice with the Energy Production and Infrastructure Center (EPIC), UNC Charlotte, for three years, where she taught at undergraduate and graduate levels. Her background is in power systems controls, with an emphasis on modeling, analysis, planning, and AI-based optimization. Her current research interests include distributed controls and secure control frameworks under uncertainty, applications on energy system modeling, stochastic optimization, and electric vehicle, including electric and hybrid-electric and ESSs.

CHRISTOPHER S. EDRINGTON (Senior Member, IEEE) received the B.S. degree in engineering from Arkansas State University, in 1999, and the M.S. and Ph.D. degrees in electrical engineering from the Missouri University of Science and Technology, in 2001 and 2004, respectively. He was a fellow of GAANN and IGERT with the Missouri University of Science and Technology. From 2004 to 2007, he was an Assistant Professor in electrical engineering with the College of Engineering, Arkansas State University. From 2007 to 2019, he held the ranks of an Assistant Professor, an Associate Professor, and a Full Professor in electrical and computer engineering with the FAMU-FSU College of Engineering and was the Lead of the Energy Conversion and Integration Thrust, Florida State University-Center for Advanced Power Systems. In 2019, he joined Clemson University as the Warren H. Owen Distinguished Professor in electrical and computer engineering, where he leads the Real-Time COntrol and Optimization Laboratory (RT-COOL). He is currently the Associate Director of Industry Relations with the VIPR-GS Center, Clemson University. His research interests include modeling, simulation, optimization and control of: electromechanical drive systems, applied power electronics, integration of renewable energy, storage, pulse power loads, and hardware in the loop (HIL) VV&A experimentation.